Title	**Lagrangian transport induced by peristaltic pumping in a tube**
Author(s)	**Ma, Y; Ng, CO**
Citation	**Fluid Dynamics Research, 2011, v. 43 n. 1**
Issued Date	**2011**
URL	**http://hdl.handle.net/10722/129260**
Rights	**Creative Commons: Attribution 3.0 Hong Kong License**

Lagrangian transport induced by peristaltic pumping in a tube

Ye Ma and Chiu-On Ng

Department of Mechanical Engineering,
The University of Hong Kong, Pokfulam Road, Hong Kong

Fax: (852) 2858 5415
E-mail: cong@hku.hk

September 1, 2010

Abstract

This is an analytical study, based on equations of motion in Lagrangian form, for the steady Lagrangian fluid transport induced by long peristaltic waves (which can be progressive, purely or partially standing) of small amplitude traveling on the boundary of a flexible tube. The first-order oscillatory viscous flow and the higher-order time-mean Lagrangian drifts (or steady streaming) are obtained as functions of the wave properties. Two cases are considered. First, the wave frequency is slow such that the steady-streaming Reynolds number (Re_s) is very small and the viscous diffusion is significant across the entire flow region. The time-mean flow can be found in the second-order problem. Second, high frequency pumping is considered such that $Re_s = O(1)$. Under this condition, the flow domain is divided into a thin Stokes boundary layer near the wall and the inviscid core region. The steady streaming in the core region is to be found in the fourth-order problem. Based on the Lagrangian coordinates, all the solutions are analytically expressed. Results are generated to illustrate the effects of wave properties on the Lagrangian transport. The phenomenon of reflux, a backward time-mean flow, is examined in particular.

1 Introduction

Physiologically, peristaltic pumping is an inherent neuromuscular property of a biological system in which bio-fluids are transported along a tube by the propulsive movements of the tube wall. The ureter passes urine by peristalsis from the kidney to the bladder against an adverse pressure gradient. Other physiological processes, such as chyme flow and food mixing in the gastrointestinal tract, the movement of ova in the Fallopian tube, the movement of spermatozoa in the efferent ducts of the male reproductive tract, and the vasomotion of the small blood vessels in circulation, are all based on peristaltic transport (Ali *et al* 2009).

A classical paper on peristalsis is due to Fung and Yih (1968). By a perturbation analysis, they deduced a theory for the backward time-mean flow called reflux, which is a pathological phenomenon in ureter flow leading to possible bacteria transport from the bladder to the kidneys. They found that there would be no reflux if the pressure gradient was below a certain critical value. Peristaltic pumping of finite amplitude but without inertia was then examined by Shapiro *et al* (1969). The phenomena and general properties of reflux and trapping were described and elucidated in detail by these authors. The early body of literature on peristalsis was reviewed by Jaffrin and Shapiro (1971). Based on the lubrication approximation, other effects germane to the biological environments were examined in subsequent studies, such as long peristaltic waves of arbitrary profiles (Manton 1975), unsteady flow in a semi-infinite tube with one end closed and the other end open (Uchida and Aoki 1977), viscoelastic (Bohme and Friedrich 1983) and non-Newtonian (Provost and Schwarz 1994) fluid, a peripheral viscous layer (Brasseur and Corrsin 1987) or a compliant wall (Haroun 2006), and more recently the boundary slip effects (Ali *et al* 2009). Most of these analytical works are limited by the conditions of small steady-streaming Reynolds numbers or low-frequency oscillations.

The present work aims to examine the steady Lagrangian drifts (or Lagrangian steady streaming) of Newtonian fluid particles contained in a flexible tube under the action of small-amplitude peristaltic waves imposed on the boundary of the tube. Based on the conditions that the wave amplitude is much smaller than the tube radius and the wavelength is much longer than the tube radius, a perturbation analysis is

performed so that the first-order solutions are purely first harmonics in time, while the time-independent solutions are obtained in the second or higher orders. Also by a perturbation approach, Wang and Tarbell (1992, 1995) studied the steady streaming induced by an oscillatory pressure gradient, when the steady-streaming Reynolds number, $Re_s = (\epsilon\alpha)^2$, is either very small or very large, where ϵ is a small parameter representing the ratio of wave amplitude a to the tube radius h, and $\alpha = h(\sigma/\nu)^{1/2} = \sqrt{2}h/\delta$ is known as the Womersley number, in which σ is the angular frequency of wave, ν is the kinematic viscosity of fluid, and $\delta = (2\nu/\sigma)^{1/2}$ is the Stokes layer thickness. In the case of finite steady-streaming Reynolds numbers, $a \sim \delta$ or $Re_s = O(1)$, for which convection and viscous diffusion are equally important in the transport of second-order vorticity from the Stokes boundary layer into the inviscid core of the flow field, the analytical solution is not available in the existing literature.

Ma and Ng (2009) studied the steady streaming induced by a pressure-driven wave propagating through a prestressed viscoelastic tube, also by the Lagrangian description, when $a \ll \delta$. Practically, in many physiological systems, ϵ is in the range of $0.01-0.2$ and the Womersley number can be as high as 50 (Olsen and Shapiro 1967, Jaffrin and Shapiro 1971, Wilmer and Michael 1998). Hence, the condition of finite steady-streaming Reynolds numbers $Re_s = O(1)$ is of practical significance and needs to be studied in detail. Based on the Lagrangian approach, the present model can yield purely analytical solutions for Lagrangian mass transport under the condition $Re_s \leq O(1)$. This is in sharp contrast to the Eulerian problem which has to be solved numerically when $Re_s = O(1)$ (Wang and Tarbell 1992). The present problem formulation is similar to that by Ng and Ma (2009), who studied the Lagrangian transport induced by peristalsis in a closed two-dimensional channel. Here, our focus is on the effects of standing wave and return current on the peristaltic time-mean flow through a partially obstructed tube.

This paper is organized as follows. The problem is formulated in terms of Lagrangian coordinates as detailed in §2, where the small length ratio ϵ is used as an ordering parameter for the problem. Following previous studies (e.g. Barton and Raynor 1968, Manton 1975, Wang and Tarbell 1992, 1995), the long wave approximation is adopted here. On expanding the equations and variables in terms of the small parameter, a perturbation analysis is performed. In §3.1, solutions to the first-order

motions, which are purely time-oscillatory, are developed. In §3.2, the second-order time-mean motions are found. There are two components of the steady streaming: one-dimensional and cellular components, arising from different modes of interactions between the forward and backward waves traveling on the tube wall. In §4, the case of fast oscillation such that $\alpha \sim \epsilon^{-1} \gg 1$ or $Re_s = O(1)$ is looked into. This is a case in which the flow domain is divided into the boundary layer and the core region. Near the tube wall is a thin Stokes boundary layer in which the second-order steady vorticity is generated. The transport of the vorticity into the core region is accomplished by means of convection as well as viscous diffusion in the present case where the wave amplitude is comparable with the Stokes layer thickness. In this fast-oscillation case, the steady streaming velocity has to be found in the fourth-order problem, requiring the second- and third-harmonic solutions to be derived first. It turns out that, for this particular problem, the fourth-order forcing terms balance each other exactly and the steady Lagrangian velocities in the core are determined only by the second-order time-mean velocities at the outer edge of the boundary layer. Hence, the fast-oscillation mass transport has the same structure whether the steady-streaming Reynolds number is equal to or smaller than order unity. Finally, some discussions on the effects of the controlling parameters (the Womersley number, the backward wave amplitude and phase angle, and the return current) on the Lagrangian transport are presented in §5.

2 Problem Formulation

We consider flow induced by peristaltic pumping of an incompressible Newtonian viscous fluid contained in a long flexible tube of radius h and length L. Fully-developed axisymmetrical flow is assumed. By Lagrangian description, the instantaneous radial and axial positions of a fluid particle (r, z) are functions of the undisturbed coordinates (R, Z) and time t. The origin $R = 0$ is set at a point in the center of the tube, and the flexible wall is initially located at $R = h$; see figure 1. Fluid motion is caused by a partial standing wave resulting from the superposition of two peristaltic waves propagating in opposite directions on the flexible tube wall at $R = h$:

$$r(h, Z, t) = \eta(Z, t) = a\mathrm{Re}\left[\mathrm{e}^{\mathrm{i}(kZ-\sigma t)} + S\mathrm{e}^{\mathrm{i}(kZ+\sigma t)}\right], \tag{1}$$

where Re denotes the real part, i is the complex unit, a is the amplitude of the forward wave, k is the wavenumber, and σ is the angular frequency of the waves, $S = S_r e^{i\phi}$ is the complex amplitude of the backward wave with magnitude S_r and phase angle ϕ. All these wave parameters are prescribed quantities. The wave is in general a partial standing wave with $0 < S_r < 1$. In the two limits, the wave becomes purely progressive when $S_r = 0$, and purely standing when $S_r = 1$. For $S_r > 0$, ϕ represents the phase difference between the forward wave and the backward wave.

It is further assumed that the wavelength is of the order of the tube length L, i.e. $kL = O(1)$, and is much larger than the tube radius h. For long waves of small amplitude, the following parameter

$$\epsilon \equiv a/h \sim h/L \ll 1 \tag{2}$$

will be used as the ordering parameter in the following analysis. The equations of motion and boundary conditions in Lagrangian form are obtainable from Ma and Ng (2009), and are recalled as follows. Using the standard notation for the Jacobian, the mass conservation equation is

$$\frac{\partial(r,z)}{\partial(R,Z)} = \frac{R}{r}, \tag{3}$$

and the r- and z-momentum equations are

$$\epsilon^2 \ddot{r} = -\frac{r}{\rho R}\frac{\partial(p,z)}{\partial(R,Z)} + \frac{\epsilon^2}{\rho}\left[\frac{1}{R}\frac{\partial(r\tau_{rr},z)}{\partial(R,Z)} + \frac{r}{R}\frac{\partial(r,\tau_{rz})}{\partial(R,Z)} - \frac{\tau_{\theta\theta}}{r}\right], \tag{4}$$

$$\ddot{z} = -\frac{r}{\rho R}\frac{\partial(r,p)}{\partial(R,Z)} + \frac{1}{\rho}\left[\frac{1}{R}\frac{\partial(r\tau_{zr},z)}{\partial(R,Z)} + \epsilon^2\frac{r}{R}\frac{\partial(r,\tau_{zz})}{\partial(R,Z)}\right], \tag{5}$$

and the stress components are

$$\tau_{rr} = 2\mu\frac{r}{R}\frac{\partial(\dot{r},z)}{\partial(R,Z)}, \tag{6}$$

$$\tau_{\theta\theta} = 2\mu\frac{\dot{r}}{r}, \tag{7}$$

$$\tau_{zz} = 2\mu\frac{r}{R}\frac{\partial(r,\dot{z})}{\partial(R,Z)}, \tag{8}$$

and

$$\tau_{rz} = \tau_{zr} = \mu\frac{r}{R}\left[\epsilon^2\frac{\partial(r,\dot{r})}{\partial(R,Z)} + \frac{\partial(\dot{z},z)}{\partial(R,Z)}\right]. \tag{9}$$

In the equations above, an overdot is used to denote time derivative, p is the pressure, ρ is the fluid density, and μ is the dynamic viscosity. Gravity is ignored. The small parameter ϵ is inserted for identification of the relative order of the associated term.

The symmetry boundary condition is used at the tube axis:

$$\dot{r} = 0, \quad \frac{\partial \dot{z}}{\partial R} = 0 \qquad \text{on } R = 0. \tag{10}$$

On the tube surface, the particles undergo motion in the radial direction only

$$\dot{r} = \dot{\eta}, \quad \dot{z} = 0 \qquad \text{on } R = h, \tag{11}$$

where η is given in equation (1).

On the basis of small-amplitude displacements, the variables may be expanded as follows:

$$(r, z, p) = (R, Z, 0) + \epsilon \left(r^{(1)}, z^{(1)}, p^{(1)}\right) + \epsilon^2 \left(r^{(2)}, z^{(2)}, p^{(2)}\right) + \cdots. \tag{12}$$

Perturbation equations are obtainable for the $O(\epsilon)$ and $O(\epsilon^2)$ variables on substituting equation (12) into the Lagrangian equations above and collecting terms of equal powers of ϵ.

3 Slow Oscillation

3.1 First-Order Problem

Solutions to the first-order problem can be found by first separating the variables into components due to the forward and backward propagating waves:

$$\left(r^{(1)}, z^{(1)}, p^{(1)}\right) = \mathrm{Re}\left\{(\tilde{r}, \tilde{z}, \tilde{p})\, \mathrm{e}^{\mathrm{i}(kZ - \sigma t)} + S\,(\tilde{r}^*, -\tilde{z}^*, \tilde{p}^*)\, \mathrm{e}^{\mathrm{i}(kZ + \sigma t)}\right\}, \tag{13}$$

where an asterisk is used to denote complex conjugate, $\tilde{r}$ and $\tilde{z}$ are functions of β, $\tilde{p}$ is an unknown constant to be determined by the boundary conditions. On substituting the expressions above into the $O(\epsilon)$ equations, the first-order solutions can be written as

$$\tilde{z}(R) = \mathrm{i}kA_1 + \lambda J_0(\lambda R) A_2, \tag{14}$$

$$\tilde{r}(R) = \frac{k^2 R}{2} A_1 - \mathrm{i}k J_1(\lambda R) A_2, \tag{15}$$

$$\tilde{p} = \sigma^2 \rho A_1, \tag{16}$$

where J_n is the Bessel function of the first kind of order n,

$$\lambda^2 = \mathrm{i}\sigma/\nu = 2\mathrm{i}/\delta^2, \tag{17}$$

in which

$$\delta = \sqrt{2\nu/\sigma} \tag{18}$$

is the Stokes layer thickness. At this point, we assume that $\delta \sim h$ so that the viscous effect is significant across the entire tube section. The case of very small Stokes layer thickness will be considered in §4.

On using the $O(\epsilon)$ boundary conditions, the constant A_1 and A_2 can be determined as follows:

$$A_1 = \frac{2a\lambda J_0(\lambda h)}{k^2\left[\lambda h J_0(\lambda h) - 2J_1(\lambda h)\right]}, \tag{19}$$

$$A_2 = \frac{2a}{\mathrm{i}k\left[\lambda h J_0(\lambda h) - 2J_1(\lambda h)\right]}. \tag{20}$$

3.2 Second-Order Problem

The second-order flow field considered here is for a general oscillation frequency such that the Stokes layer thickness is comparable with the tube radius, $\delta \sim h$; the steady-streaming Reynolds number is, however, small such that $a \ll \delta$.

The $O(\epsilon^2)$ governing equations are as follows:

$$\frac{\partial z^{(2)}}{\partial Z} + \frac{\partial r^{(2)}}{\partial R} + \frac{r^{(2)}}{R} = \frac{r^{(1)} r^{(1)}}{R^2} + \frac{\partial r^{(1)}}{\partial Z}\frac{\partial z^{(1)}}{\partial R} - \frac{\partial z^{(1)}}{\partial Z}\frac{\partial r^{(1)}}{\partial R}, \tag{21}$$

$$\frac{1}{\rho}\frac{\partial p^{(2)}}{\partial R} = G^{(2)}, \tag{22}$$

$$\ddot{z}^{(2)} + \frac{1}{\rho}\frac{\partial p^{(2)}}{\partial Z} - \nu\left(\frac{\partial^2 \dot{z}^{(2)}}{\partial R^2} + \frac{1}{R}\frac{\partial \dot{z}^{(2)}}{\partial R}\right) = H^{(2)}, \tag{23}$$

where the forcing terms can be decomposed into inviscid and viscous parts: $G^{(2)} = G_I^{(2)} + G_V^{(2)}$ and $H^{(2)} = H_I^{(2)} + H_V^{(2)}$, which are given in equations (A.1)–(A.4). All these forcing terms, which consist of products of the first-order variables, are responsible for the generation of steady currents in the second order.

The steady component of the Lagrangian drift is called the mass transport velocity in water waves (Longuet-Higgins 1953). Let us define

$$(u,\, v) \equiv \left(\bar{\dot{z}}^{(2)}, \bar{\dot{r}}^{(2)}\right), \tag{24}$$

where the overbar denotes time average over a period. Suppose time is long enough for a steady field of Lagrangian streaming to be fully established along the entire tube. The mass transport velocity components are governed by the time-averaged $O(\epsilon^2)$ equations (21)–(23), which read as below:

$$\frac{\partial u}{\partial Z} + \frac{\partial v}{\partial R} + \frac{v}{R} = 0, \tag{25}$$

$$\frac{1}{\rho}\frac{\partial \bar{p}^{(2)}}{\partial R} = \bar{G}^{(2)}, \tag{26}$$

and

$$\frac{1}{\rho}\frac{\partial \bar{p}^{(2)}}{\partial Z} - \nu\left[\frac{\partial^2 u}{\partial R^2} + \frac{1}{R}\frac{\partial u}{\partial R}\right] = \bar{H}^{(2)}. \tag{27}$$

The time-mean forcing terms can be separated into two parts, the first part being independent of Z, and the second part being proportional to $\exp(2\mathrm{i}kZ)$:

$$\left(\bar{G}^{(2)}, \bar{H}^{(2)}\right) = \left(\tilde{G}, \tilde{H}\right) + \mathrm{Re}\left\{\left(\tilde{\tilde{G}}, \tilde{\tilde{H}}\right)\mathrm{e}^{2\mathrm{i}kZ}\right\}, \tag{28}$$

where $\tilde{G}$, $\tilde{H}$, $\tilde{\tilde{G}}$ and $\tilde{\tilde{H}}$, which are functions of R only, are given in equations (A.5)–(A.8).

We may accordingly decompose the time-mean variables into

$$\left(u, v, \bar{p}^{(2)}\right) = \left(\tilde{U}, 0, \tilde{P}\right) + \mathrm{Re}\left\{\left(\tilde{\tilde{U}}, \tilde{\tilde{V}}, \tilde{\tilde{P}}\right)\mathrm{e}^{2\mathrm{i}kZ}\right\}, \tag{29}$$

where $\tilde{U}$, $\tilde{\tilde{U}}$, $\tilde{\tilde{V}}$ and $\tilde{\tilde{P}}$ are pure functions of R, while $\tilde{P}$ is a linear function of Z such that $\partial\tilde{P}/\partial Z$ is a constant. Obviously, the first and the second parts on the right hand side of equation (29) represent components of the steady flow field which are axially uniform (one dimensional with parallel streamlines) and axially periodic (two dimensional with cellular recirculating streamlines), respectively.

3.2.1 One-dimensional steady streaming

We may infer from equation (26) that the mean pressure gradient $\partial\tilde{P}/\partial Z$ does not depend on R, and it is in fact a constant pressure gradient responsible for the generation of a return current (Ünlüata and Mei 1970). Hence, the flow is governed by, from equation (27),

$$\nu\frac{(R\tilde{U}')'}{R} = -\tilde{H} + \rho^{-1}\frac{\partial\tilde{P}}{\partial Z}, \tag{30}$$

which can be solved by integration twice with respect to R. The two integration constants and the pressure gradient $\partial\tilde{P}/\partial Z$ are determined using the boundary conditions $\tilde{U}'(0) = \tilde{U}(h) = 0$, and the volume-flux condition $\langle\tilde{U}\rangle = 0$ if the tube is completely closed at its ends, or $\partial\tilde{P}/\partial Z = 0$ if the tube is completely open at its ends (Ünlüata and Mei 1970). After some algebra, we get

$$\begin{aligned}\tilde{U}(R) &= \rho^{-1}\frac{\partial\tilde{P}}{\partial Z}\frac{(R^2-h^2)}{4\nu} - \frac{1-|S|^2}{2}\mathrm{Re}\Bigg\{3\mathrm{i}\sigma k^2\lambda A_1^* A_2\left[J_0(\lambda R) - J_0(\lambda h)\right] \\ &\quad + \frac{2\mathrm{i}\sigma^3 k|A_2|^2}{\nu^2}\int_h^R \frac{1}{R}\int_0^R R\left|J_0(\lambda R)\right|^2 \mathrm{d}R\,\mathrm{d}R \\ &\quad - \frac{3\sigma^3 k|A_2|^2}{\nu^2}\int_h^R \frac{1}{R}\int_0^R R\left|J_1(\lambda R)\right|^2 \mathrm{d}R\,\mathrm{d}R\Bigg\}, \end{aligned} \tag{31}$$

and

$$\begin{aligned}\rho^{-1}\frac{\partial\tilde{P}}{\partial Z} &= -Y\frac{8(1-|S|^2)\nu}{h^4}\mathrm{Re}\Bigg\{3\mathrm{i}\sigma k^2 h A_1^* A_2\left[J_1(\lambda h) - \frac{\lambda h J_0(\lambda h)}{2}\right] \\ &\quad + \frac{2\mathrm{i}\sigma^3 k|A_2|^2}{\nu^2}\int_0^h R\int_h^R \frac{1}{R}\int_0^R R\left|J_0(\lambda R)\right|^2 \mathrm{d}R\,\mathrm{d}R\,\mathrm{d}R \\ &\quad - \frac{3\sigma^3 k|A_2|^2}{\nu^2}\int_0^h R\int_h^R \frac{1}{R}\int_0^R R\left|J_1(\lambda R)\right|^2 \mathrm{d}R\,\mathrm{d}R\,\mathrm{d}R\Bigg\}, \end{aligned} \tag{32}$$

where $0 \le Y \le 1$ is a numerical factor corresponding to the degree of end obstruction of the tube. At the two limits,

$$Y = \begin{cases} 0 & \text{if the tube is completely open,} \\ 1 & \text{if the tube is completely closed,} \end{cases} \tag{33}$$

while in general $0 < Y < 1$ represents a partially obstructed tube. If the wave becomes purely standing, $S = 1$, recirculating cells will be formed and the volume-flux is zero across any section in the tube irrespective of Y.

3.2.2 Cellular steady streaming

Equations (25)–(27) give

$$2ik\tilde{\tilde{U}} + \tilde{\tilde{V}}' + \frac{\tilde{\tilde{V}}}{R} = 0, \tag{34}$$

$$\rho^{-1}\tilde{\tilde{P}}' = \tilde{\tilde{G}}, \tag{35}$$

$$2ik\rho^{-1}\tilde{\tilde{P}} - \nu\left[\tilde{\tilde{U}}'' + \frac{\tilde{\tilde{U}}'}{R}\right] = \tilde{\tilde{H}}. \tag{36}$$

Using the boundary conditions $\tilde{\tilde{U}}'(0) = 0$, $\tilde{\tilde{U}}(h) = 0$, $\tilde{\tilde{V}}(0) = 0$ and $\tilde{\tilde{V}}(h) = 0$, the equations above can be solved as follows:

$$\begin{aligned}
\tilde{\tilde{U}}(R) &= (-\mathrm{i}S)\Bigg[\frac{4g_1(R^2-h^2)}{h^4} - \frac{3k^2\sigma^2}{\nu}\mathrm{Im}\left\{\frac{A_1^* A_2\left[J_0(\lambda R) - J_0(\lambda h)\right]}{\lambda}\right\} \\
&\quad - \frac{2\sigma^2 k|A_2|^2}{\nu}\int_h^R \frac{1}{R}\int_0^R \mathrm{Re}\left\{(\mathrm{i}\lambda^* + \lambda)J_0(\lambda R)J_1^*(\lambda R)\right\}\mathrm{d}R\,\mathrm{d}R \\
&\quad + \frac{3\sigma^3 k|A_2|^2}{\nu^2}\int_h^R \frac{1}{R}\int_0^R R\left|J_0(\lambda R)\right|^2\mathrm{d}R\,\mathrm{d}R \\
&\quad + \frac{4\sigma^2 k|A_2|^2}{\nu}\int_h^R \frac{1}{R}\int_0^R \frac{\left|J_1(\lambda R)\right|^2}{R}\mathrm{d}R\,\mathrm{d}R\Bigg], \qquad (37)
\end{aligned}$$

$$\begin{aligned}
\tilde{\tilde{V}}(R) &= S\Bigg[-\frac{2kg_1R(R^2-2h^2)}{h^4} + \frac{6k^3\sigma^2}{\nu}\mathrm{Im}\left\{\frac{A_1^* A_2}{\lambda}\left[\frac{J_1(\lambda R)}{\lambda} - \frac{J_0(\lambda h)R}{2}\right]\right\} \\
&\quad + \frac{4\sigma^2k^2|A_2|^2}{R\nu}\int_0^R R\int_h^R \frac{1}{R}\int_0^R \mathrm{Re}\left\{(\mathrm{i}\lambda^* + \lambda)J_0(\lambda R)J_1^*(\lambda R)\right\}\mathrm{d}R\,\mathrm{d}R\,\mathrm{d}R \\
&\quad - \frac{6\sigma^3k^2|A_2|^2}{R\nu^2}\int_0^R R\int_h^R \frac{1}{R}\int_0^R R\left|J_0(\lambda R)\right|^2\mathrm{d}R\,\mathrm{d}R\,\mathrm{d}R \\
&\quad - \frac{8\sigma^2k^2|A_2|^2}{R\nu}\int_0^R R\int_h^R \frac{1}{R}\int_0^R \frac{\left|J_1(\lambda R)\right|^2}{R}\mathrm{d}R\,\mathrm{d}R\,\mathrm{d}R\Bigg], \qquad (38)
\end{aligned}$$

where g_1 is given in (A.9). Again, one may check that the inviscid forcings $\tilde{\tilde{G}}_I$ and $\tilde{\tilde{H}}_I$ give a zero right-hand side of equation (36) with the substitution of equation (35), and hence do not contribute to the cellular transport velocity field as well.

4 Fast Oscillation

Let us examine the case when the oscillation frequency is so high that the Stokes layer thickness becomes comparable with the wave amplitude: $\delta \sim a \ll h$, or the steady-streaming Reynolds number $Re_s = O(1)$. Under this condition, the flow domain can be divided into two regions: boundary layer close to the wall and the core region. The viscous flow is now confined largely to the Stokes boundary layer, which is much smaller than the tube radius. The sharp contrast in length scales is now extended to $|\lambda| \sim \delta^{-1} \gg h^{-1}$ or $|\lambda h| \sim \epsilon^{-1} \gg 1$. As a result of change of the orders of terms, the analysis, especially for the steady streaming flow, needs to be modified.

4.1 First-order solution

Applying the boundary layer approximations, namely $1/R \ll \partial/\partial R$, the governing equations can be simplified. In the core region, the viscous terms are negligible. By matching the velocities at the edge of the Stokes boundary layer, we obtain the composite periodic solution at $O(\epsilon)$:

$$\tilde{z}(R) = A_3 \left[1 - \mathrm{e}^{\mathrm{i}\lambda(h-R)}\right], \tag{39}$$

$$\tilde{r}(R) = -\frac{\mathrm{i}kA_3}{2}R, \tag{40}$$

$$\tilde{p} = -\frac{\mathrm{i}\rho\sigma^2 A_3}{k}, \tag{41}$$

where $A_3 = 2a\mathrm{i}/(kh)$. The term $\exp[\mathrm{i}\lambda(h-R)]$ in equation (39) is only significant in the boundary layer, and the oscillatory axial velocity in the core region has a uniform profile.

4.2 Higher-order solutions

4.2.1 Boundary layer

Using the boundary layer approximations, $1/R \ll \partial/\partial R$ again, equations (25)–(27) can be simplified to yield

$$\frac{\partial u_{bl}}{\partial Z} + \frac{\partial v_{bl}}{\partial R} = 0, \tag{42}$$

$$\frac{1}{\rho}\frac{\partial \bar{p}_{bl}^{(2)}}{\partial R} = \bar{G}_{bl}^{(2)}, \tag{43}$$

and

$$\frac{1}{\rho}\frac{\partial \bar{p}_{bl}^{(2)}}{\partial Z} - \nu\frac{\partial^2 u_{bl}}{\partial R^2} = \bar{H}_{bl}^{(2)}, \tag{44}$$

where the subscript bl is used to denote a boundary-layer quantity. With the separation into components by equations (28) and (29), the governing equations are

$$\nu\tilde{U}_{bl}'' = -\tilde{H}_{bl} \tag{45}$$

for the one-dimensional steady streaming, and

$$\nu\tilde{\tilde{U}}_{bl}'' = 2\mathrm{i}k\int \tilde{\tilde{G}}_{bl}\mathrm{d}R - \tilde{\tilde{H}}_{bl}, \qquad \tilde{\tilde{V}}_{bl} = -2\mathrm{i}k\int \tilde{\tilde{U}}_{bl}\mathrm{d}R \tag{46}$$

for the cellular steady streaming. Source terms that are dominant in the boundary layer can be identified from equations (A.6)–(A.8) as

$$\tilde{H}_{bl} = -\tfrac{1}{2}(1-|S|^2)\nu\sigma k\left[4\mathrm{Re}\left\{\tilde{z}\tilde{z}^{*\prime\prime}\right\} + 3\left|\tilde{z}^{\prime}\right|^2\right], \tag{47}$$

$$\tilde{\tilde{G}}_{bl} = -S\sigma^2\mathrm{Re}\left\{\tilde{z}^{\prime}\tilde{z}^{*}\right\} + S\nu\sigma\mathrm{Im}\left\{\tilde{z}^{\prime}\tilde{z}^{*\prime\prime}\right\}, \tag{48}$$

$$\tilde{\tilde{H}}_{bl} = (-\mathrm{i}S)\sigma^2 k|\tilde{z}|^2 - 4(-\mathrm{i}S)\nu\sigma k\mathrm{Im}\left\{\tilde{z}\tilde{z}^{*\prime\prime}\right\}. \tag{49}$$

We get from equations (45) and (47) the one-dimensional mass transport velocity in the bottom boundary layer:

$$\tilde{U}_{bl}(R) = (1-|S|^2)\left[\frac{8\sigma^2a^2}{\nu kh^2}\mathrm{Im}\left\{\frac{\mathrm{e}^{\mathrm{i}\lambda(h-R)}}{\lambda^2}\right\} + \frac{3\sigma a^2}{kh^2}\mathrm{e}^{\mathrm{i}(\lambda-\lambda^*)(h-R)}\right] + \tilde{U}_{bl}^{\infty}, \tag{50}$$

where

$$\tilde{U}_{bl}^{\infty} = (1-|S|^2)\frac{5\sigma a^2}{kh^2} \tag{51}$$

is the steady Lagrangian drift at the outer edge of the boundary layer. The boundary conditions $\tilde{U}_{bl}(h) = \tilde{U}_{bl}^{\prime}(\infty) = 0$ have been used. Here, infinity means a sufficiently large distance from the boundary layer.

For the cellular steady streaming, we get from equations (46), (48) and (49) its mass transport velocity components in the boundary layer:

$$\begin{aligned}\tilde{\tilde{U}}_{bl}(R) &= (-\mathrm{i}S)\left[\frac{4a^2\sigma^2}{\nu kh^2}\mathrm{Re}\left\{\frac{\mathrm{e}^{\mathrm{i}\lambda(h-R)}}{\lambda^2}\right\}\right.\\ &\left. + \frac{12a^2\sigma}{kh^2}\mathrm{Im}\left\{\mathrm{e}^{\mathrm{i}\lambda(h-R)} + \frac{\mathrm{i}\mathrm{e}^{\mathrm{i}(\lambda-\lambda^*)(h-R)}}{2}\right\}\right] + \tilde{\tilde{U}}_{bl}^{\infty},\end{aligned} \tag{52}$$

$$\begin{aligned}\tilde{\tilde{V}}_{bl}(R) &= S\left[\frac{8a^2\sigma^2}{\nu h^2}\mathrm{Re}\left\{\frac{\mathrm{e}^{\mathrm{i}\lambda(h-R)}}{\mathrm{i}\lambda^3}\right\}\right.\\ &\left. + \frac{24a^2\sigma}{h^2}\mathrm{Im}\left\{\frac{\mathrm{e}^{\mathrm{i}\lambda(h-R)}}{\mathrm{i}\lambda} + \frac{\mathrm{e}^{\mathrm{i}(\lambda-\lambda^*)(h-R)}}{2(\lambda-\lambda^*)}\right\}\right] + \tilde{\tilde{V}}_{bl}^{\infty},\end{aligned} \tag{53}$$

where

$$\tilde{\tilde{U}}_{bl}^{\infty} = \mathrm{i}S\frac{6a^2\sigma}{kh^2}, \tag{54}$$

$$\tilde{\tilde{V}}_{bl}^{\infty} = S\left[\frac{32a^2\sigma}{h^2}\mathrm{Re}\left\{\frac{1}{\lambda}\right\} - \frac{12a^2\sigma}{h^2}\mathrm{Im}\left\{\frac{1}{\lambda-\lambda^*}\right\}\right] \tag{55}$$

are the components of the cellular Lagrangian drifts at the outer edge of the boundary layer. The conditions of zero velocity at the wall and zero velocity gradient far from the boundary layer are also applied.

4.2.2 Core region

The viscous effect becomes subdominant in the core region. One can check that the viscous stress and source terms in equations (22) and (23) are now two orders of magnitude smaller than other terms in the $O(\epsilon^2)$ equations. Hence, the second-order equations contain only the inviscid terms:

$$\frac{1}{\rho}\frac{\partial p^{(2)}}{\partial R} = G_I^{(2)}, \tag{56}$$

$$\ddot{z}^{(2)} + \frac{1}{\rho}\frac{\partial p^{(2)}}{\partial Z} = H_I^{(2)}, \tag{57}$$

where $G_I^{(2)}$ and $H_I^{(2)}$ are given in equations (A.1) and (A.3).

The third-order equations are also without the viscous terms:

$$\begin{aligned}\frac{\partial z^{(3)}}{\partial Z} + \frac{\partial r^{(3)}}{\partial R} + \frac{r^{(3)}}{R} \;=\; & \frac{\partial z^{(1)}}{\partial R}\frac{\partial r^{(2)}}{\partial Z} + \frac{\partial r^{(1)}}{\partial Z}\frac{\partial z^{(2)}}{\partial R} - \frac{\partial z^{(1)}}{\partial Z}\frac{\partial r^{(2)}}{\partial R} - \frac{\partial r^{(1)}}{\partial R}\frac{\partial z^{(2)}}{\partial Z} \\ & - \left(\frac{r^{(1)}}{R}\right)^3 + 2\frac{r^{(1)}r^{(2)}}{R^2},\end{aligned} \tag{58}$$

$$\frac{1}{\rho}\frac{\partial p^{(3)}}{\partial R} = -\ddot{r}^{(1)}, \tag{59}$$

$$\ddot{z}^{(3)} + \frac{1}{\rho}\frac{\partial p^{(3)}}{\partial Z} = -\left(\ddot{z}^{(2)} + \frac{\partial z^{(1)}}{\partial Z}\ddot{z}^{(1)}\right)\frac{\partial z^{(1)}}{\partial Z} + \ddot{z}^{(1)}\left(\frac{\partial r^{(2)}}{\partial R} + \frac{r^{(2)}}{R} + \frac{r^{(1)}}{R}\frac{\partial r^{(1)}}{\partial R}\right). \tag{60}$$

The steady streaming can then be found from the fourth-order momentum equations, in which the second-order viscous terms show up:

$$\ddot{r}^{(2)} + \rho^{-1}\frac{\partial p^{(4)}}{\partial R} = \rho^{-1}G_I^{(4)} + G_V^{(2)}, \tag{61}$$

$$\ddot{z}^{(4)} + \rho^{-1}\frac{\partial p^{(4)}}{\partial Z} - \nu\left(\frac{\partial^2 \dot{z}^{(2)}}{\partial R^2} + \frac{1}{R}\frac{\partial \dot{z}^{(2)}}{\partial R}\right) = \rho^{-1}H_I^{(4)} + H_V^{(2)}, \tag{62}$$

where $G_V^{(2)}$, $H_V^{(2)}$, $G^{(4)}$, $H^{(4)}$ are given in equations (A.2), (A.4), (A.10), and (A.11), respectively. Upon taking time-average of these equations, we get

$$\rho^{-1}\frac{\partial \bar{p}^{(4)}}{\partial R} = \rho^{-1}\bar{G}_I^{(4)} + \bar{G}_V^{(2)}, \tag{63}$$

$$\rho^{-1}\frac{\partial \bar{p}^{(4)}}{\partial Z} - \nu\left(\frac{\partial^2 u}{\partial R^2} + \frac{1}{R}\frac{\partial u}{\partial R}\right) = \rho^{-1}\bar{H}_I^{(4)} + \bar{H}_V^{(2)}. \tag{64}$$

When compared with the counterpart equations (26) and (27), these equations for the steady Lagrangian drifts contain additional forcing terms that are products of first-, second- and third-order variables.

The second-order variables can be found by solving equations (21), (56) and (57), where their right-hand sides are computed using the first-order inviscid solutions given in equations (39)–(40). The time-oscillatory parts of the second-order solution can be obtained as follows:

$$\left(z^{(2)}, r^{(2)}, p^{(2)}\right) = \mathrm{Re}\left\{\left(z^{(21)}, 0, p^{(21)}\right)\mathrm{e}^{2\mathrm{i}(kZ-\sigma t)} + \left(z^{(22)}, 0, p^{(22)}\right)\mathrm{e}^{2\mathrm{i}(kZ+\sigma t)}\right\}, \tag{65}$$

where

$$z^{(21)} = \tfrac{3}{16}\mathrm{i}kA_3^2, \quad \rho^{-1}p^{(21)} = \tfrac{5}{8}\sigma^2 A_3^2, \tag{66}$$

$$z^{(22)} = \tfrac{3}{16}\mathrm{i}kS^2A_3^{*2}, \quad \rho^{-1}p^{(22)} = \tfrac{5}{8}\sigma^2 S^2 A_3^{*2}. \tag{67}$$

The third-order variables are obtained likewise by solving equations (58)–(60) with the boundary conditions $r^{(3)}(0) = r^{(3)}(h) = 0$. Only the first-harmonic components may give rise to a non-zero time-mean when interacting with the first-order variables. These components are of the following modes:

$$\begin{aligned}\left(z^{(3)}, r^{(3)}, p^{(3)}\right) \;=\; & \mathrm{Re}\Big\{\left(z^{(31)}, r^{(31)}, p^{(31)}\right)\mathrm{e}^{\mathrm{i}(kZ-\sigma t)} + \left(z^{(32)}, r^{(32)}, p^{(32)}\right)\mathrm{e}^{\mathrm{i}(kZ+\sigma t)} \\ & + \left(z^{(33)}, 0, p^{(33)}\right)\mathrm{e}^{\mathrm{i}(3kZ-\sigma t)} + \left(z^{(34)}, 0, p^{(34)}\right)\mathrm{e}^{\mathrm{i}(3kZ+\sigma t)} \\ & + \mathrm{hht}\Big\},\end{aligned} \tag{68}$$

where hht stands for higher-harmonic terms. After some algebra, $z^{(31)}$, $r^{(31)}$, $p^{(31)}$, $z^{(32)}$, $r^{(32)}$ and $p^{(32)}$ are found as functions of R, while $z^{(33)}$, $p^{(33)}$, $z^{(34)}$ and $p^{(34)}$ are constants. The expressions of them are given in equations (A.12)–(A.21).

We may now evaluate the forcing terms on the right-hand sides of equations (61) and (62) for the steady streaming. With $\partial p^{(1)}/\partial R = \partial p^{(2)}/\partial R = \partial z^{(1)}/\partial R = \partial z^{(2)}/\partial R = r^{(2)} = 0$, one can get that $G_V^{(2)} = H_V^{(2)} = 0$. Hence, the second-order viscous forcing terms do not contribute to the steady streaming. The forcing only comprises the fourth-order inviscid interaction terms, which can be expressed as:

$$G_I^{(4)} = \frac{\partial p^{(1)}}{\partial Z}\frac{\partial z^{(3)}}{\partial R} + \frac{\partial p^{(3)}}{\partial R}\frac{\partial r^{(1)}}{\partial R}, \tag{69}$$

$$H_I^{(4)} = \frac{\partial p^{(3)}}{\partial R}\frac{\partial r^{(1)}}{\partial Z} - \frac{\partial p^{(1)}}{\partial Z}\left(\frac{\partial r^{(3)}}{\partial R} + \frac{r^{(3)}}{R}\right) + \frac{\partial p^{(3)}}{\partial Z}\frac{\partial z^{(1)}}{\partial Z} - \frac{\partial p^{(2)}}{\partial Z}\frac{r^{(1)}}{R}\frac{\partial r^{(1)}}{\partial R}, \tag{70}$$

whose time-average can be further expressed as

$$\left(\bar{G}_I^{(4)}, \bar{H}_I^{(4)}\right) = \left(\tilde{G}_I^{(4)}, \tilde{H}_I^{(4)}\right) + \mathrm{Re}\left[\left(\tilde{\tilde{G}}_I^{(4)}, \tilde{\tilde{H}}_I^{(4)}\right)\mathrm{e}^{2\mathrm{i}kZ}\right] + \mathrm{Re}\left[\left(0, \tilde{\tilde{H}}_I^{(4)}\right)\mathrm{e}^{4\mathrm{i}kZ}\right], \tag{71}$$

where $\tilde{G}_I^{(4)}$, $\tilde{H}_I^{(4)}$, $\tilde{\tilde{G}}_I^{(4)}$, and $\tilde{\tilde{H}}_I^{(4)}$ are given in equations (A.22)–(A.25). $\tilde{\tilde{H}}_I^{(4)}$ is a constant which will only give rise to a steady pressure gradient in the axial direction but not the steady streaming of particles.

We may accordingly decompose the time-mean variables into

$$\left(u, v, \bar{p}^{(4)}\right) = \left(\tilde{U}_c, 0, \tilde{P}_c\right) + \mathrm{Re}\left[\left(\tilde{\tilde{U}}_c, \tilde{\tilde{V}}_c, \tilde{\tilde{P}}_c\right)\mathrm{e}^{2\mathrm{i}kZ}\right] + \mathrm{Re}\left[\left(0, 0, \tilde{\tilde{P}}_c\right)\mathrm{e}^{4\mathrm{i}kZ}\right]. \tag{72}$$

The one-dimensional Lagrangian drift in the core is governed by:

$$\nu\frac{(R\tilde{U}_c')'}{R} = -\tilde{H}_I^{(4)} + \rho^{-1}\frac{\partial \tilde{P}_c}{\partial Z}, \tag{73}$$

where $\partial\tilde{P}_c/\partial Z$ is a constant. The cellular Lagrangian drift in the core is now governed by

$$2ik\tilde{\tilde{U}}_c + \tilde{\tilde{V}}_c' + \frac{\tilde{\tilde{V}}_c}{R} = 0, \tag{74}$$

$$\tilde{\tilde{P}}_c' = \tilde{\tilde{G}}_I^{(4)}, \tag{75}$$

$$2ik\rho^{-1}\tilde{\tilde{P}}_c - \nu\left[\tilde{\tilde{U}}_c'' + \frac{\tilde{\tilde{U}}_c'}{R}\right] = \rho^{-1}\tilde{\tilde{H}}_I^{(4)}. \tag{76}$$

After some algebra on the substitution of the second- and third-order oscillatory quantities into equations (A.23)–(A.25), the source terms are simplified to

$$\tilde{H}_I^{(4)} = 0, \tag{77}$$

$$\tilde{\tilde{G}}_I^{(4)} = -\frac{1}{4}\left\{\sigma^2\rho k^2 S|A_3|^2 R\right\}, \tag{78}$$

$$\tilde{\tilde{H}}_I^{(4)} = -\frac{\sigma^2\rho k^3|A_3|^2}{16}\left\{4\mathrm{i}S\left(R^2 - h^2\right) + \mathrm{i}S\left(7 - 4|S|^2\right)|A_3|^2\right\}. \tag{79}$$

One can readily find that the forcing terms in equation (76) that are functions of R cancel those from equation (75), leaving behind a constant term that determines only the axial pressure gradient but not the velocity. On matching the velocity components

at the outer edge of the boundary layer, $\tilde{U}_c(h) = \tilde{U}_{bl}^{\infty}$, $\tilde{\tilde{U}}_c(h) = \tilde{\tilde{U}}_{bl}^{\infty}$ and $\tilde{\tilde{V}}_c(h) = \tilde{\tilde{V}}_{bl}^{\infty}$, the time-mean variables can be found in a similar manner as before:

$$\tilde{U}_c(R) = \rho^{-1}\frac{\partial \tilde{P}_c}{\partial Z}\frac{(R^2-h^2)}{4\nu} + \tilde{U}_{bl}^{\infty}, \qquad \rho^{-1}\frac{\partial \tilde{P}_c}{\partial Z} = Y\frac{8\nu}{h^2}\tilde{U}_{bl}^{\infty}, \tag{80}$$

$$\tilde{\tilde{U}}_c(R) = \frac{(2R^2-h^2)}{h^2}\tilde{\tilde{U}}_{bl}^{\infty} + \frac{2\mathrm{i}\,(h^2-R^2)}{kh^3}\tilde{\tilde{V}}_{bl}^{\infty}, \tag{81}$$

$$\tilde{\tilde{V}}_c(R) = \frac{\mathrm{i}kR(h^2-R^2)}{h^2}\tilde{\tilde{U}}_{bl}^{\infty} + \frac{R\,(2h^2-R^2)}{h^3}\tilde{\tilde{V}}_{bl}^{\infty}. \tag{82}$$

After a rather tedious course of deriving the steady streaming solutions under fast oscillation, one finds that the time-mean flow in the core region is eventually determined simply by the second-order time-mean velocities at the outer edge of the boundary layer; the fourth-order inviscid forcing terms balance themselves exactly and have no net contributions to the Lagrangian transport. It is interesting to note that the solutions obtained above, which are good for $\epsilon^2 \sim \alpha^{-2} \ll 1$ (wave amplitude comparable to the Stokes layer thickness), are the same as those obtained simply by solving the second-order time-averaged viscous equations under the condition $\epsilon^2 \ll \alpha^{-2} \ll 1$ (wave amplitude much smaller than the Stokes layer thickness). Therefore, for the present problem, the solutions for high Womersley numbers are the same whether the steady-streaming Reynolds number is less than or equal to order unity. This result would not be known without having gone through the higher-order perturbation analysis presented above.

Finally, the Lagrangian transport velocities which are uniformly valid across the whole fluid region are given by

$$\begin{aligned}
\tilde{U}(R) &= \tilde{U}_c(R) + \tilde{U}_{bl}(R) - \tilde{U}_{bl}^{\infty} \\
&= \left[1 + Y\frac{2\,(R^2-h^2)}{h^2}\right]\tilde{U}_{bl}^{\infty} \\
&\quad + (1-|S|^2)\left[\frac{8\sigma^2a^2}{\nu kh^2}\mathrm{Im}\left\{\frac{\mathrm{e}^{\mathrm{i}\lambda(h-R)}}{\lambda^2}\right\} + \frac{3\sigma a^2}{kh^2}\mathrm{e}^{\mathrm{i}(\lambda-\lambda^*)(h-R)}\right],
\end{aligned} \tag{83}$$

for the one-dimensional steady streaming, and

$$\begin{aligned}
\tilde{\tilde{U}}(R) &= \tilde{\tilde{U}}_c(R) + \tilde{\tilde{U}}_{bl}(R) - \tilde{\tilde{U}}_{bl}^{\infty} \\
&= \frac{(2R^2-h^2)}{h^2}\tilde{\tilde{U}}_{bl}^{\infty} + \frac{2\mathrm{i}\,(h^2-R^2)}{kh^3}\tilde{\tilde{V}}_{bl}^{\infty} + (-\mathrm{i}S)\left[\frac{4a^2\sigma^2}{\nu kh^2}\mathrm{Re}\left\{\frac{\mathrm{e}^{\mathrm{i}\lambda(h-R)}}{\lambda^2}\right\}\right. \\
&\quad \left. + \frac{12a^2\sigma}{kh^2}\mathrm{Im}\left\{\mathrm{e}^{\mathrm{i}\lambda(h-R)} + \frac{\mathrm{i}\mathrm{e}^{\mathrm{i}(\lambda-\lambda^*)(h-R)}}{2}\right\}\right],
\end{aligned} \tag{84}$$

$$
\begin{aligned}
\tilde{\hat{V}}(R) &= \tilde{\hat{V}}_c(R) + \tilde{\hat{V}}_{bl}(R) - \tilde{\hat{V}}_{bl}^{\infty} \\
&= \frac{\mathrm{i}kR(h^2-R^2)}{h^2}\tilde{\hat{U}}_{bl}^{\infty} + \frac{R\,(2h^2-R^2)}{h^3}\tilde{\hat{V}}_{bl}^{\infty} + S\left[\frac{8a^2\sigma^2}{\nu h^2}\mathrm{Re}\left\{\frac{\mathrm{e}^{\mathrm{i}\lambda(h-R)}}{\mathrm{i}\lambda^3}\right\}\right. \\
&\quad \left. + \frac{24a^2\sigma}{h^2}\mathrm{Im}\left\{\frac{\mathrm{e}^{\mathrm{i}\lambda(h-R)}}{\mathrm{i}\lambda} + \frac{\mathrm{e}^{\mathrm{i}(\lambda-\lambda^*)(h-R)}}{2(\lambda-\lambda^*)}\right\}\right]
\end{aligned}
\tag{85}
$$

for the cellular steady streaming.

5 Discussions

The problems and expressions deduced above can be non-dimensionalized using the following normalization scheme, where the normalized quantities are distinguished by an overhead caret:

$$
\left.
\begin{array}{l}
\hat{t} = \sigma t, \quad (\hat{R},\hat{\delta}) = (R,\delta)/h, \quad \left(\hat{Z},k\right) = \left(Z,\hat{k}\right)/L, \quad \alpha = \lambda h/\sqrt{\mathrm{i}} \\
\hat{A}_1 = A_1/\left(aL^2/h\right) \quad \hat{A}_2 = A_2/\left(aL\right), \quad \partial\tilde{\hat{P}}/\partial\hat{Z} = \partial\tilde{P}/\partial Z/\left(\rho\sigma a^2 L\nu/h^4\right) \\
\left(\tilde{\hat{U}}_{bl}^{\infty}, \tilde{\hat{\hat{U}}}_{bl}^{\infty}, \hat{\tilde{U}}, \tilde{\hat{\hat{U}}}\right) = \left(\tilde{U}_{bl}^{\infty}, \tilde{\hat{U}}_{bl}^{\infty}, \tilde{U}, \tilde{\hat{U}}\right)/\left(\sigma a^2 L/h^2\right), \quad \hat{g}_1 = g_1/\left(\sigma a^2 L\right) \\
\left(\hat{\tilde{V}}_{bl}^{\infty}, \tilde{\hat{\hat{V}}}_{bl}^{\infty}, \hat{\tilde{V}}, \tilde{\hat{\hat{V}}}\right) = \left(\tilde{V}_{bl}^{\infty}, \tilde{\hat{V}}_{bl}^{\infty}, \tilde{V}, \tilde{\hat{V}}\right)/\left(\sigma a^2/h\right),
\end{array}
\right\}
\tag{86}
$$

where the Womersley number is introduced to represent the significance of the oscillation frequency.

The primary variables of interest are the second-order time-mean variables

$$
(\hat{u},\hat{v}) = \left(\hat{\tilde{U}} + \mathrm{Re}\left[\left(\tilde{\hat{\hat{U}}}, \tilde{\hat{\hat{V}}}\right)\mathrm{e}^{2\mathrm{i}\hat{k}\hat{Z}}\right]\right), \tag{87}
$$

which are functions of $(\hat{R},\hat{Z})$. The controlling parameters are the wavelength $\hat{k}$, the Womersley number α, the backward wave amplitude S with magnitude S_r and phase angle ϕ, and the parameter Y for the end condition.

The Womersley number $\alpha = \sqrt{2}h/\delta$ can be interpreted as a ratio of the tube radius to the Stokes layer thickness; the higher the frequency, the larger the Womersley number. The steady-streaming Reynolds number is here defined to be $Re_s \equiv (\epsilon\alpha)^2$. We reiterate that the results presented in §3.2 are good for order unity $\hat{\delta}$, or $\alpha = O(1)$, as long as $Re_s \ll 1$ or $a \ll \delta \sim h$, while those presented in §4 are valid for $\alpha \sim \epsilon^{-1} \gg 1$, $Re_s = O(1)$, or $a \sim \delta \ll h$. The ratio of the wave amplitude to the

tube radius $\epsilon = a/h$ in physiological systems is in the range of $0.01 - 0.2$ (Olsen and Shapiro 1967, Jaffrin and Shapiro 1971). We here consider the value $\epsilon = 0.05$, such that the results in §3.2 are only valid when $\alpha < 10$, while for $\alpha \geq 10$, the results in §4 are used. We also remark that the normalization scale for the second-order velocities is $\sigma a^2/h = Re_s(\nu/h)$, and hence the basic dependence of these velocities on Re_s is already taken into account by the normalization. Therefore, when normalized, the steady streaming is independent of Re_s under all conditions.

Some numerical results, which are obtained with the computational package Mathcad Version 14, are presented here to further examine the effects of the controlling parameters on the time-mean velocities. Figure 2 shows the effect of the Womersley number on the Lagrangian transport velocity, where the wave is partially standing, $S_r = 0.7, \phi = \pi/3$ and the tube end is partially open, $Y = 0.5$. When the oscillation frequency is small, $\alpha = 1$, the transport velocity is almost one-dimensional in the axial direction and significant in the core region of the tube. However, as the frequency increases, say $\alpha = 5$, the cellular steady streaming becomes appreciable in the whole fluid region, but the flow close to the outer wall is still weak. Four recirculation cells are formed over one wavelength and one cell is in the opposite direction to the adjacent one. The boundary layer phenomenon will clearly show up as the frequency goes higher; see figure 2(c) and (d). A sharp interface with one-dimensional flow can be seen between the boundary layer and the core region. The distance between the interface and the tube wall is almost three times the Stokes layer thickness δ. When under fast oscillation, the vorticity generated by viscous diffusion is largely confined within the boundary layer, which in turn induces the mass transport velocity in the core region. As a result, the magnitude of the steady streaming close to the wall is comparable to that in the core. Results shown in figure 2 can be interpreted in the context of transport of fluid parcels in the ureteral flow, or chyme flow in the gastro-intestinal tract. Parcels could be easily transported downstream at low frequencies. As the frequency increases, parcels would be trapped in the core region of the tube and the peristaltic mixing is enhanced due to the standing wave. In practice, the shape of the ureter during peristalsis is far from sinusoidal (Manton 1975). The harmonics of the sinusoidal peristaltic waves can be achieved by Fourier transformation. Therefore, the actual parcel transport velocity during peristalsis can be obtained by the summation of all the individual steady streaming velocities at each

mode of harmonics with different frequencies as shown in figure 2.

Figures 3 and 4 show the streamlines for time-mean velocities as a function of the backward wave amplitude S_r and phase angle ϕ, respectively, under fast oscillation condition ($\alpha = 20$), when the tube is partially open ($Y = 0.5$). The stream function ψ can be calculated directly from the velocity fields:

$$\frac{\partial \psi}{\partial \hat{R}} = \hat{R}\hat{u}, \qquad \frac{\partial \psi}{\partial \hat{Z}} = -\hat{R}\hat{v}. \tag{88}$$

For a pure progressive wave $S_r = 0$, the mass transport field is strictly one-dimensional (i.e. purely axial). A pure standing wave is established on the other limit $S_r = 1$, as illustrated in figure 3(d). One may find that the steady velocity components, $\hat{\bar{U}}, \hat{\bar{\bar{U}}}, \hat{\bar{\bar{V}}}$ can be expressed as

$$\left(\hat{\bar{U}}, \hat{\bar{\bar{U}}}, \hat{\bar{\bar{V}}}\right) = \left[\left(1 - |S|^2\right)\hat{\bar{U}}_r(\hat{R}), -\mathrm{i}S\hat{\bar{\bar{U}}}_r(\hat{R}), S\hat{\bar{\bar{V}}}_r(\hat{R})\right], \tag{89}$$

where $\hat{\bar{U}}_r(\hat{R})$, $\hat{\bar{\bar{U}}}_r(\hat{R})$ and $\hat{\bar{\bar{V}}}_r(\hat{R})$ are real functions of $\hat{R}$ only and are independent of the backward wave amplitude coefficient S for both the slow and fast oscillation solutions. Since $S = S_r \mathrm{e}^{\mathrm{i}\phi}$, the expression above can again be used to show that the strength of the backward wave is responsible for enhancing the cellular steady streaming pattern and suppressing the one-dimensional component of the steady flow. While the mass transport velocity pattern is much affected by the amplitude of the backward wave, the phase angle will only have the trivial effect of shifting the entire flow pattern axially (figure 4). The actual boundary motion of the peristaltic waves in the ureteral flow or chyme flow in the intestine is not as simple as the present one which is the superposition of two peristaltic waves propagating in opposite directions. Its motion is controlled by the muscle contraction which may not be determined in advance. However, the amplitude and the phase angle of backward wave could be adjusted in some artificial peristaltic pumps according to the requirements of the clinical surgery.

We further show in figure 5 how the obstruction parameter Y influences the steady transport velocities in partially standing waves under fast oscillation condition $\alpha = 20$. We recall that $Y = 0$ corresponds to zero mean pressure gradient $\partial \hat{\bar{\bar{P}}}_c / \partial \hat{Z}$ as in an open tube, and $Y = 1$ corresponds to zero volume flux as in a closed tube. In practice, the constant Y should be determined from the conditions at the ends of the tube.

For example, in the ureter problem, the end conditions are determined by the kidney and the ureterovesical junction with the bladder such that Y varies depending on the ureteral disease state. The factor Y is only responsible for diminishing the one-dimensional steady streaming (the condition of zero volume flux is always satisfied in the cellular steady streaming), such that the cellular flow will become dominant in the flow as Y increases, as shown in figure 5(a)–(c). However, when Y further increases ($Y = 1$ in figure 5(d)), the return current will induce a backward streaming flow in the tube core and push the circulation cells towards the boundary wall.

Figure 6 shows the steady axial velocity profile $\hat{\bar{U}}(\hat{R})$ as a function of the Womersley number α and the obstruction parameter Y, where the applied peristaltic wave is a purely progressive wave ($S_r = 0$). It can be seen that when Re_s is small, say $\alpha = 1$ or 5, there is a mean flux in the negative axial direction in a layer of fluid near the tube wall although the volume flux across the whole cross-section is positive ($Y < 1$). This phenomenon was discovered previously by Shapiro *et al* (1969) and Manton (1975). As $Re_s = O(1)$, the backward streaming flow will show up in the tube core, and the flow near the wall keeps positive, as illustrated in figure 6(c). We remark that as long as $S_r \leq 1$, the axial steady velocity at the outer edge of the boundary layer is always positive and independent of α, which in turn determines a parabolic and frequency-independent axial velocity profile in the core region. The one-dimensional component of the steady velocity becomes minimum at the centerline. This explains why a negative steady flow shows up close to the tube center at the high frequency limit. Reflux always happens in the 'hydro-ureter' which is a swollen ureter with much increased lumen filled with urine (Fung 1990). In the 'hydro-ureter' case, the peristaltic motion becomes a traveling wave of relatively small amplitude and the efficiency of pumping is decreased a lot. Under reflux conditions, bacteria would pass from the bladder to the kidney in a direction opposite to the mean discharge, leading to diseases such as tuberculosis and interstitial cystitis. It becomes clear from the current results that bacteria may be transported backwards to the kidney along the ureteral periphery when the oscillation frequency is small, while in the fast oscillation case, bacteria is transported backwards along the centerline of the ureter. Since the oscillation frequency is changeable at different clinical situations, the present solutions have the advantages to fully describe the bacteria transport in the 'hydro-ureter' at any frequencies. Previously, Wang and Tarbell (1995) presented

analytical expressions for the steady axial velocity profile at two limits: $Re_s \to 0$, where the velocity field is described exactly by Poiseuille's law with a peak value at the tube center; $Re_s \to \infty$, where the velocity field is described approximately by $\sin \pi \hat{R}^2$ with a peak velocity close to the tube wall. Here, under the condition of finite $Re_s = O(1)$ for fast oscillation, the present steady axial velocity profiles as illustrated in figure 6 are the first time that have been obtained with analytical expressions.

In their study on peristalsis in a two-dimensional channel, Fung and Yih (1968) found a critical pressure gradient above which a backward time-mean flow (reflux) would be induced. In the present work, when the oscillation frequency is slow, the point for minimum steady axial velocity $\hat{\bar{U}}(\hat{R})$ across the section is always close to the wall and the reflux will be enhanced as Y increases, as shown in figure 6. Therefore, the critical pressure gradient is the one that corresponds to a zero gradient of the one-dimensional velocity $\hat{\bar{U}}(\hat{R})$ at the wall:

$$\hat{\bar{U}}'(1) = 0 \quad \text{and} \quad \hat{\bar{U}}''(1) > 0 \tag{90}$$

(the cellular streaming velocities are periodic along the tube axis and do not contribute to the reflux). In the fast oscillation case, the minimum steady axial velocity is at the tube center as discussed before. It can be easily shown that when $Y = 0.5$, $\hat{\bar{U}}$ in the core region has a simple form

$$\hat{\bar{U}}(\hat{R}) = \hat{R}^2 \hat{\bar{U}}_{bl}^{\infty}, \tag{91}$$

where the steady axial velocity becomes zero at the center as shown in figure 6(b). When $Y > 0.5$, the velocity becomes negative at the tube center. Therefore, $Y = 0.5$ is the critical value, above which reflux will happen in the tube core. Further, the critical pressure can be found as

$$\left.\frac{\partial \hat{\bar{P}}_c}{\partial \hat{Z}}\right|_{\text{critical}} = 4\hat{\bar{U}}_{bl}^{\infty}. \tag{92}$$

It is interesting to note that the critical pressure gradient is a function of the oscillation frequency in the slow oscillation case, but not in the fast oscillation problem, since the parabolic steady axial velocity profile in the core is only determined by the steady velocity at the outer edge of the boundary layer which is independent of frequency as discussed before.

6 Concluding remarks

In this work, we have studied the steady Lagrangian transport induced by small-amplitude, long peristaltic waves applied on the boundary of a flexible tube, where the resultant wave can vary between the limits of a progressive wave and a standing wave, and the domain can vary between the limits of an open tube and a closed tube. Here, the problem is entirely Lagrangian in formulation and analysis. Under the conditions that the Womersley number is order unity but the steady-streaming Reynolds number is low (i.e. the Stokes layer thickness is comparable with the tube radius, but is much greater than the wave amplitude), the steady streaming velocities have been solved in the second order by the perturbation analysis. The time-mean flow is found to consist of the one-dimensional and the cellular components. When the frequency is so high that the Stokes layer thickness becomes comparable with the wave amplitude, the time-mean velocities can also be found in a rigorous manner by solving the time-averaged fourth-order problem. It turns out that for this particular problem, the solutions corresponding to large Womersley numbers are the same whether the steady-streaming Reynolds number is smaller than or equal to order unity. This simplicity in result may come as no surprise since under long waves the fluid motion is predominantly in the axial direction, and hence is only weakly affected by the inertia. This conclusion would not be made if the problem is carried out by Eulerian description or without the long wave assumption.

In summary, our model is purely analytical and is valid to small or finite steady-streaming Reynolds numbers $Re_s \leq O(1)$. Our model yields explicit expressions for simple, straightforward and efficient calculations of Lagrangian drifts under the conditions of slow or fast oscillations. The present Lagrangian model for fast oscillation is not limited to peristalsis problems, but can be extended to other wave-induced bio-fluid transport problems, e.g. blood flow in arteries and gas flow in pulmonary airways.

The imposed pressure gradient is absent, which is called 'free pumping' in the present model (Fung and Yih 1968). In practical (e.g. ureteral) peristalsis, when the bladder is full and its pressure is high, a negative pressure gradient will be imposed on the peristaltic pumping. The inclusion of the imposed pressure gradient could be

one extension of the present work. On the other hand, based on the perturbation analysis, the present work is limited by the condition of small-amplitude peristaltic waves. When the wave amplitude becomes large, another phenomenon, viz. trapping, in peristaltic pumping will show up. As the trapping happens (usually when ϵ is larger than 0.5), some streamlines will diverge to enclose a bolus of fluid particles and the bolus will moves as a whole with the wave speed (Shapiro *et al* 1969). People usually studied trapping by either totally neglecting the inertia effect (Shapiro *et al* 1969, Manton 1975, Ali *et al* 2009) or numerical simulations (Takabatake *et al* 1988). In future work, it is worthwhile to numerically solve the peristaltic pumping by the Lagrangian coordinates which have the advantage of being able to describe conditions on the moving boundary exactly. The phenomenon of trapping and the effects of non-Newtonian fluid, wall compliance and slip boundary effect deserve to be examined in detail.

Acknowledgments

The financial support by the Research Grants Council of the Hong Kong Special Administrative Region, China, through Project No. HKU 715609E is gratefully acknowledged. This study constitutes part of the work performed by the first author for his Ph.D. thesis under the supervision of the second author at the University of Hong Kong.

Appendix. Terms in the equations

In equations (21)–(23),

$$G_I^{(2)} = -\ddot{z}^{(1)}\frac{\partial z^{(1)}}{\partial R}, \tag{A.1}$$

$$G_V^{(2)} = \nu\left[\frac{\partial z^{(1)}}{\partial R}\frac{\partial^2 \dot{z}^{(1)}}{\partial R^2} + \frac{1}{R}\frac{\partial z^{(1)}}{\partial R}\frac{\partial \dot{z}^{(1)}}{\partial R}\right], \tag{A.2}$$

$$H_I^{(2)} = -\ddot{z}^{(1)}\frac{\partial z^{(1)}}{\partial Z}, \tag{A.3}$$

$$\begin{aligned} H_V^{(2)} = \nu\Bigg[&-\frac{\partial}{\partial R}\left(\frac{\partial r^{(1)}}{\partial R}\frac{\partial \dot{z}^{(1)}}{\partial R} + \frac{\partial z^{(1)}}{\partial R}\frac{\partial \dot{z}^{(1)}}{\partial Z}\right) - \frac{1}{R}\left(\frac{\partial r^{(1)}}{\partial R}\frac{\partial \dot{z}^{(1)}}{\partial R} + \frac{\partial z^{(1)}}{\partial R}\frac{\partial \dot{z}^{(1)}}{\partial Z}\right) \\ &- \frac{\partial r^{(1)}}{\partial R}\frac{\partial^2 \dot{z}^{(1)}}{\partial R^2} - \frac{\partial z^{(1)}}{\partial R}\frac{\partial^2 \dot{z}^{(1)}}{\partial R \partial Z} - \frac{r^{(1)}}{R^2}\frac{\partial \dot{z}^{(1)}}{\partial R} \\ &+ \frac{\partial z^{(1)}}{\partial Z}\frac{\partial^2 \dot{z}^{(1)}}{\partial R^2} + \frac{1}{R}\frac{\partial z^{(1)}}{\partial Z}\frac{\partial \dot{z}^{(1)}}{\partial R}\Bigg]. \end{aligned} \tag{A.4}$$

In equation (28),

$$\tilde{G} = \tilde{G}_I + \tilde{G}_V = \tfrac{1}{2}\sigma^2(1+|S|^2)\mathrm{Re}\left\{\tilde{z}'\tilde{z}^*\right\} - \tfrac{1}{2}\nu\sigma(1+|S|^2)\mathrm{Im}\left\{\tilde{z}'\tilde{z}^{*\prime\prime}\right\}, \tag{A.5}$$

$$\begin{aligned} \tilde{H} &= \tilde{H}_V \\ &= \tfrac{1}{2}(1-|S|^2)\nu\sigma\Bigg[-k\mathrm{Re}\left\{\tilde{z}\tilde{z}^{*\prime\prime} + \frac{\tilde{z}\tilde{z}^{*\prime} + 2\left(R\tilde{z}'\tilde{z}^*\right)'}{R}\right\} \\ &\qquad + \mathrm{Im}\left\{\left(\tilde{r}^{*\prime} - \frac{\tilde{r}^*}{R}\right)\left(\frac{\tilde{z}'}{R} - \tilde{z}''\right)\right\} - k\left|\tilde{z}'\right|^2\Bigg], \end{aligned} \tag{A.6}$$

$$\tilde{\tilde{G}} = \tilde{\tilde{G}}_I + \tilde{\tilde{G}}_V = -S\sigma^2\mathrm{Re}\left\{\tilde{z}'\tilde{z}^*\right\} + S\nu\sigma\mathrm{Im}\left\{\tilde{z}'\tilde{z}^{*\prime\prime}\right\}, \tag{A.7}$$

$$\begin{aligned} \tilde{\tilde{H}} &= \tilde{\tilde{H}}_I + \tilde{\tilde{H}}_V \\ &= (-\mathrm{i}S)\sigma^2 k|\tilde{z}|^2 + (-\mathrm{i}S)\nu\sigma\Bigg[-k\mathrm{Im}\left\{\tilde{z}\tilde{z}^{*\prime\prime} + \frac{\tilde{z}\tilde{z}^{*\prime} - 2\left(R\tilde{z}'\tilde{z}^*\right)'}{R}\right\} \\ &\qquad + \mathrm{Re}\left\{\left(\tilde{r}^{*\prime} - \frac{\tilde{r}^*}{R}\right)\left(\frac{\tilde{z}'}{R} - \tilde{z}''\right)\right\}\Bigg], \end{aligned} \tag{A.8}$$

where Im stands for the imaginary part.

In equations (37) and (38),

$$\begin{aligned} g_1 &= -\frac{3k^2\sigma^2 h}{\nu}\mathrm{Im}\left\{\frac{A_1^* A_2}{\lambda}\left[\frac{J_1(\lambda h)}{\lambda}-\frac{J_0(\lambda h)h}{2}\right]\right\} \\ &\quad -\frac{2\sigma^2 k|A_2|^2}{\nu}\int_0^h R\int_h^R\frac{1}{R}\int_0^R \mathrm{Re}\left\{(\mathrm{i}\lambda^*+\lambda)J_0(\lambda R)J_1^*(\lambda R)\right\}\mathrm{d}R\,\mathrm{d}R\,\mathrm{d}R \\ &\quad +\frac{3\sigma^3 k|A_2|^2}{\nu^2}\int_0^h R\int_h^R\frac{1}{R}\int_0^R R\left|J_0(\lambda R)\right|^2\mathrm{d}R\,\mathrm{d}R\,\mathrm{d}R \\ &\quad +\frac{4\sigma^2 k|A_2|^2}{\nu}\int_0^h R\int_h^R\frac{1}{R}\int_0^R\frac{\left|J_1(\lambda R)\right|^2}{R}\mathrm{d}R\,\mathrm{d}R\,\mathrm{d}R. \end{aligned} \tag{A.9}$$

In equations (61)–(62),

$$\begin{aligned} G_I^{(4)} &= -\frac{\partial p^{(1)}}{\partial R}\left(\frac{\partial z^{(3)}}{\partial Z}+\frac{r^{(3)}}{R}+\frac{r^{(1)}}{R}\frac{\partial z^{(2)}}{\partial Z}+\frac{r^{(2)}}{R}\frac{\partial z^{(1)}}{\partial Z}\right)+\frac{\partial p^{(3)}}{\partial R}\frac{\partial r^{(1)}}{\partial R} \\ &\quad +\frac{\partial p^{(1)}}{\partial Z}\left(\frac{\partial z^{(3)}}{\partial R}+\frac{r^{(1)}}{R}\frac{\partial z^{(2)}}{\partial R}+\frac{r^{(2)}}{R}\frac{\partial z^{(1)}}{\partial R}\right)+\frac{\partial p^{(3)}}{\partial Z}\frac{\partial z^{(1)}}{\partial R} \\ &\quad -\frac{\partial p^{(2)}}{\partial R}\left(\frac{\partial z^{(2)}}{\partial Z}+\frac{r^{(2)}}{R}+\frac{r^{(1)}}{R}\frac{\partial z^{(1)}}{\partial Z}\right) \\ &\quad +\frac{\partial p^{(2)}}{\partial Z}\left(\frac{\partial z^{(2)}}{\partial Z}+\frac{r^{(1)}}{R}\frac{\partial z^{(1)}}{\partial R}\right), \end{aligned} \tag{A.10}$$

$$\begin{aligned} H_I^{(4)} &= \frac{\partial p^{(1)}}{\partial R}\left(\frac{\partial r^{(3)}}{\partial Z}+\frac{r^{(1)}}{R}\frac{\partial r^{(2)}}{\partial Z}+\frac{r^{(2)}}{R}\frac{\partial r^{(1)}}{\partial Z}\right)+\frac{\partial p^{(3)}}{\partial R}\frac{\partial r^{(1)}}{\partial Z} \\ &\quad -\frac{\partial p^{(1)}}{\partial Z}\left(\frac{\partial r^{(3)}}{\partial R}+\frac{r^{(3)}}{R}+\frac{r^{(1)}}{R}\frac{\partial r^{(2)}}{\partial R}+\frac{r^{(2)}}{R}\frac{\partial r^{(1)}}{\partial R}\right) \\ &\quad +\frac{\partial p^{(3)}}{\partial Z}\frac{\partial z^{(1)}}{\partial Z}+\frac{\partial p^{(2)}}{\partial R}\left(\frac{\partial r^{(2)}}{\partial Z}+\frac{r^{(1)}}{R}\frac{\partial r^{(1)}}{\partial Z}\right) \\ &\quad -\frac{\partial p^{(2)}}{\partial Z}\left(\frac{\partial r^{(2)}}{\partial R}+\frac{r^{(2)}}{R}+\frac{r^{(1)}}{R}\frac{\partial r^{(1)}}{\partial R}\right), \end{aligned} \tag{A.11}$$

In equation (68),

$$z^{(31)} = \tfrac{1}{8}k^2A_3(2R^2-h^2)+\tfrac{3}{16}(1+|S|^2)k^2A_3|A_3|^2, \tag{A.12}$$

$$r^{(31)} = -\tfrac{1}{16}\mathrm{i}k^3A_3R(R^2-h^2), \tag{A.13}$$

$$\rho^{-1}p^{(31)} = -\tfrac{1}{8}\sigma^2\mathrm{i}kA_3(2R^2-h^2)-\tfrac{1}{16}(12+|S|^2)\sigma^2\mathrm{i}kA_3|A_3|^2, \tag{A.14}$$

$$z^{(32)} = -\tfrac{1}{8}k^2SA_3^*(2R^2-h^2)-\tfrac{3}{16}(1+|S|^2)k^2SA_3^*|A_3|^2, \tag{A.15}$$

$$r^{(32)} = \tfrac{1}{16}\mathrm{i}k^3SA_3^*R(R^2-h^2), \tag{A.16}$$

$$\rho^{-1}p^{(32)} = \tfrac{1}{8}\sigma^2 \mathrm{i}kSA_3^*(2R^2 - h^2) - \tfrac{1}{16}(1 + 12|S|^2)\sigma^2 \mathrm{i}kSA_3^*|A_3|^2, \tag{A.17}$$

$$z^{(33)} = \tfrac{1}{16}k^2 SA_3|A_3|^2, \tag{A.18}$$

$$\rho^{-1}p^{(33)} = -\tfrac{1}{6}\sigma^2 \mathrm{i}kSA_3|A_3|^2, \tag{A.19}$$

$$z^{(34)} = -\tfrac{1}{16}k^2 S^2 A_3^*|A_3|^2, \tag{A.20}$$

$$\rho^{-1}p^{(34)} = \tfrac{1}{6}\sigma^2 \mathrm{i}kS^2 A_3^*|A_3|^2. \tag{A.21}$$

In equation (71),

$$\tilde{G}_I^{(4)} = \frac{\mathrm{Re}}{2}\left[\tfrac{1}{2}\mathrm{i}kA_3^* p^{(31)\prime} - \tfrac{1}{2}\mathrm{i}kS^* A_3 p^{(32)\prime} - \mathrm{i}kz^{(31)\prime}\tilde{p}^* - \mathrm{i}kS^* z^{(32)\prime}\tilde{p}\right], \tag{A.22}$$

$$\begin{aligned}\tilde{H}_I^{(4)} \;=\; & \frac{\mathrm{Re}}{2}\Bigg[k^2 A_3^* p^{(31)} - k^2 S^* A_3 p^{(32)} + \tfrac{1}{2}k^2 RA_3^* p^{(31)\prime} - \tfrac{1}{2}k^2 RS^* A_3 p^{(32)\prime} \\ & + \mathrm{i}k\left(r^{(31)\prime} + \frac{r^{(31)}}{R}\right)\tilde{p}^* + \mathrm{i}kS^*\left(r^{(32)\prime} + \frac{r^{(32)}}{R}\right)\tilde{p} \\ & + \tfrac{1}{4}\mathrm{i}k^3 A_3^{*2} p^{(21)} + \tfrac{1}{4}\mathrm{i}k^3 S^{*2} A_3^2 p^{(22)}\Bigg],\end{aligned} \tag{A.23}$$

$$\tilde{\tilde{G}}_I^{(4)} = \frac{1}{2}\left[-\tfrac{1}{2}\mathrm{i}kA_3 p^{(32)\prime} + \tfrac{1}{2}\mathrm{i}kSA_3^* p^{(31)\prime} + \mathrm{i}kSz^{(31)\prime}\tilde{p}^* + \mathrm{i}kz^{(32)\prime}\tilde{p}\right], \tag{A.24}$$

$$\begin{aligned}\tilde{\tilde{H}}_I^{(4)} \;=\; & \frac{1}{2}\Bigg[-k^2 A_3 p^{(32)} + k^2 SA_3^* p^{(31)} + 3k^2 A_3^* p^{(33)} - 3k^2 S^* A_3 p^{(34)} \\ & - \tfrac{1}{2}k^2 RSA_3^* p^{(31)\prime} - \mathrm{i}kS\left(r^{(31)\prime} + \frac{r^{(31)}}{R}\right)\tilde{p}^* \\ & - \mathrm{i}k\left(r^{(32)\prime} + \frac{r^{(32)}}{R}\right)\tilde{p} + \tfrac{1}{2}k^2 RA_3 p^{(32)\prime} \\ & + \tfrac{1}{2}\mathrm{i}k^3 SA_3^{*2} p^{(21)} + \tfrac{1}{2}\mathrm{i}k^3 S^* A_3^2 p^{(22)}\Bigg],\end{aligned} \tag{A.25}$$

References

Ali N, Wang Y, Hayat T and Oberlack M 2009 Slip effects on the peristaltic flow of a third grade fluid in a circular cylindrical tube *J. Appl. Mech.* **76** 011006

Barton C and Raynor S 1968 Peristaltic flow in tubes *Bull. Math. Biophys.* **30** 663–680

Bohme G and Friedrich R 1983 Peristaltic flow of viscoelastic liquids *J. Fluid Mech.* **128** 109–122

Brasseur J G and Corrsin S 1987 The influence of a peripheral layer of different viscosity on peristaltic pumping with Newtonian fluids *J. Fluid Mech.* **174** 495–519

Fung Y C and Yih C S 1968 Peristaltic transport *J. Appl. Mech.* **35** 669–675

Fung Y C 1990 *Biomechanics: Motion, Flow, Stress, and Growth*, New York, Springer-Verlag.

Jaffrin M Y and Shapiro A H 1971 Peristaltic pumping *Ann. Rev. Fluid Mech.* **3** 13–36

Haroun M H 2006 Effect of wall compliance on peristaltic transport of a Newtonian fluid in an asymmetric channel *Math. Probl. Eng.* 61475

Longuet-Higgins M S 1953 Mass transport in water waves *Phil. Trans. R. Soc. Lond. A* **245** 535–581

Ma Y and Ng C O 2009 Wave propagation and induced steady streaming in viscous fluid contained in a prestressed viscoelastic tube *Phys. Fluids* **21** 051901

Manton M J 1975 Long-wavelength peristaltic pumping at low Reynolds number *J. Fluid Mech.* **68** 467–476

Ng C O and Ma Y 2009 Lagrangian transport induced by peristaltic pumping in a closed channel *Phys. Rev. E* **80** 056307

Olsen J H and Shapiro A H 1967 Large-amplitude unsteady flow in liquid-filled elastic tube *J. Fluid Mech.* **29** 513–538

Provost A M and Schwarz W H 1994 A theoretical study of viscous effects in a peristaltic pumping *J. Fluid Mech.* **279** 177–195

Shapiro A H, Jaffrin M Y and Weinberg S L 1969 Peristaltic pumping with long wavelengths at low Reynolds number *J. Fluid Mech.* **37** 799–825

Takabatake S, Ayukawa K and Mori A 1988 Peristaltic pumping in circular cylindrical tubes: a numerical study of fluid transport and its efficiency *J. Fluid Mech.* **193** 267–283

Uchida S and Aoki R 1977 Unsteady flows in a semi-infinite contracting or expanding pipe *J. Fluid Mech.* **82** 371–387

Ünlüata Ü and Mei C C 1970 Mass transport in water waves *J. Geophys. Res.* **75** 7611–7618

Wang D M and Tarbell J M 1992 Nonlinear analysis of flow in an elastic tube (artery): steady streaming effects *J. Fluid Mech.* **239** 341–358

Wang D M and Tarbell J M 1995 Nonlinear analysis of oscillatory flow, with a nonzero mean in an elastic tube *J. Biomech. Eng.* **117** 127–135

Wilmer W N and Michael F O 1998 *McDonald's Blood Flow in Arteries: Theoretical, Experimental, and Clinical Principles*, Arnold, London.

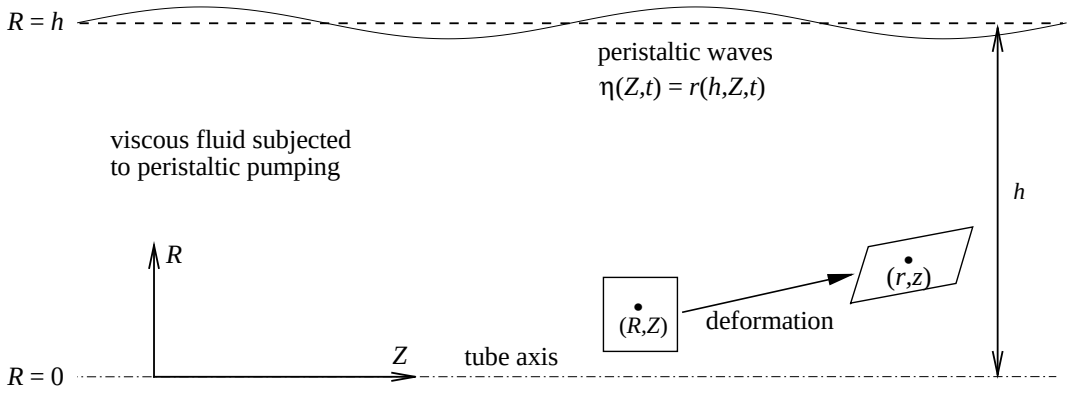

Figure 1: Definition sketch of peristaltic waves traveling on the outer boundary of a circular tube, where (R, Z) and (r, z), the Lagrangian and Eulerian coordinates, are the undisturbed and instantaneous positions of a particle.

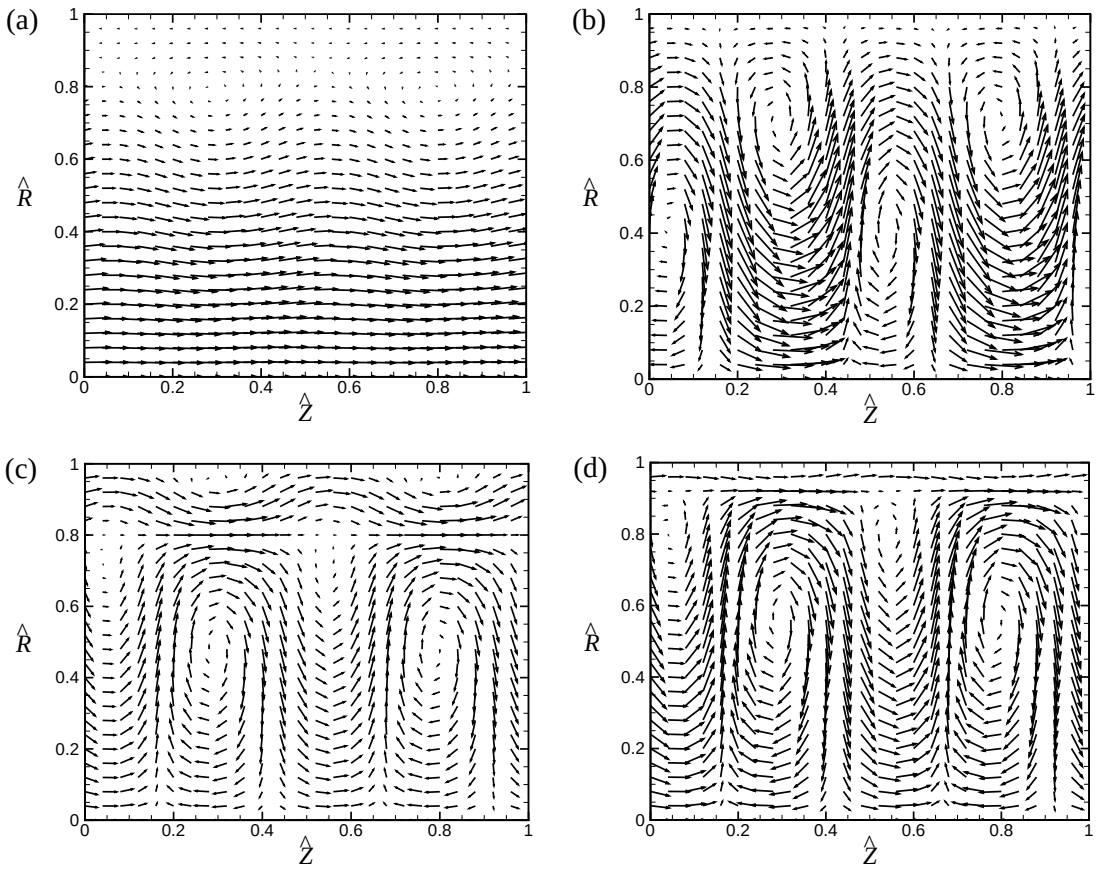

Figure 2: Effect of the wave frequency: vectors for the steady Lagrangian flow field in partially standing waves ($S_r = 0.7$, $\phi = \pi/3$) in a partially obstructed tube ($Y = 0.5$), where $\hat{k} = 2\pi$, and $\alpha =$ (a) 1, (b) 5 (c) 20, (d) 40.

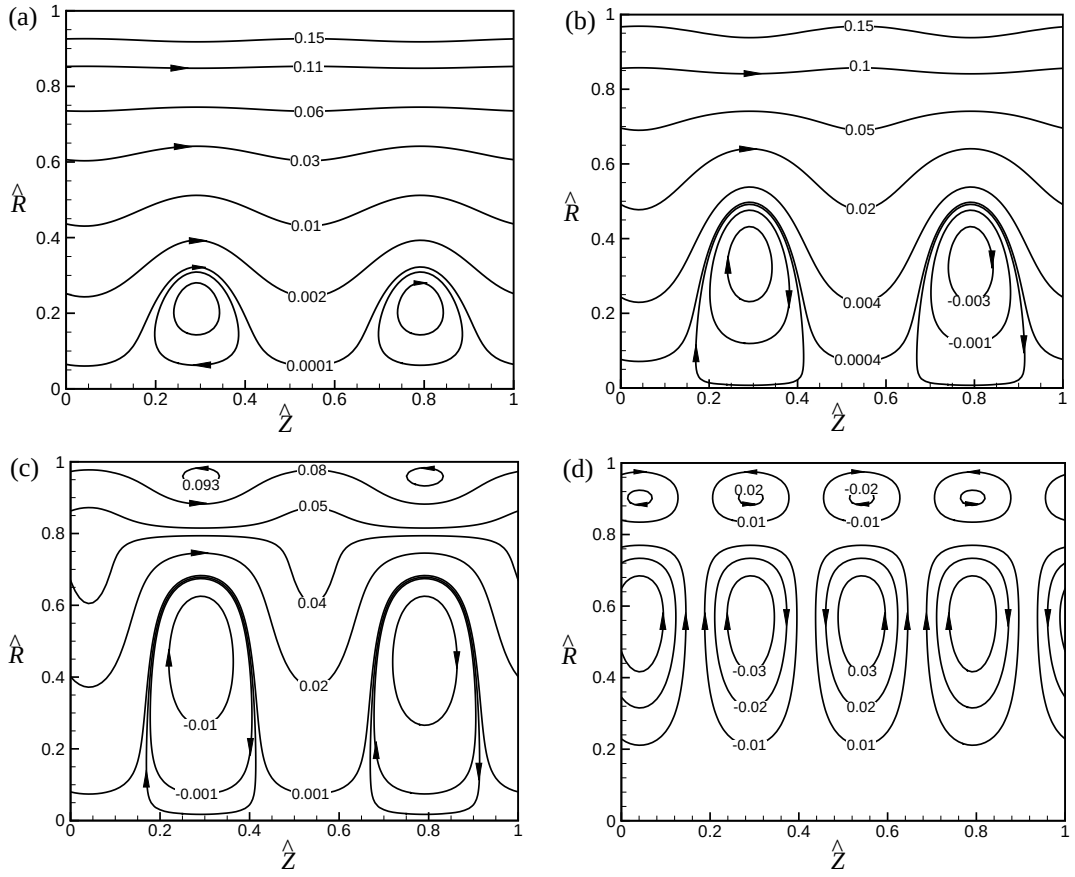

Figure 3: Effect of the magnitude of the backward wave: mass transport streamlines in partially standing waves in a partially obstructed tube ($Y = 0.5$), where $\hat{k} = 2\pi$, $\alpha = 20$, $\phi = \pi/3$ and $S_r =$ (a) 0.1, (b) 0.3 (c) 0.7, (d) 1.0.

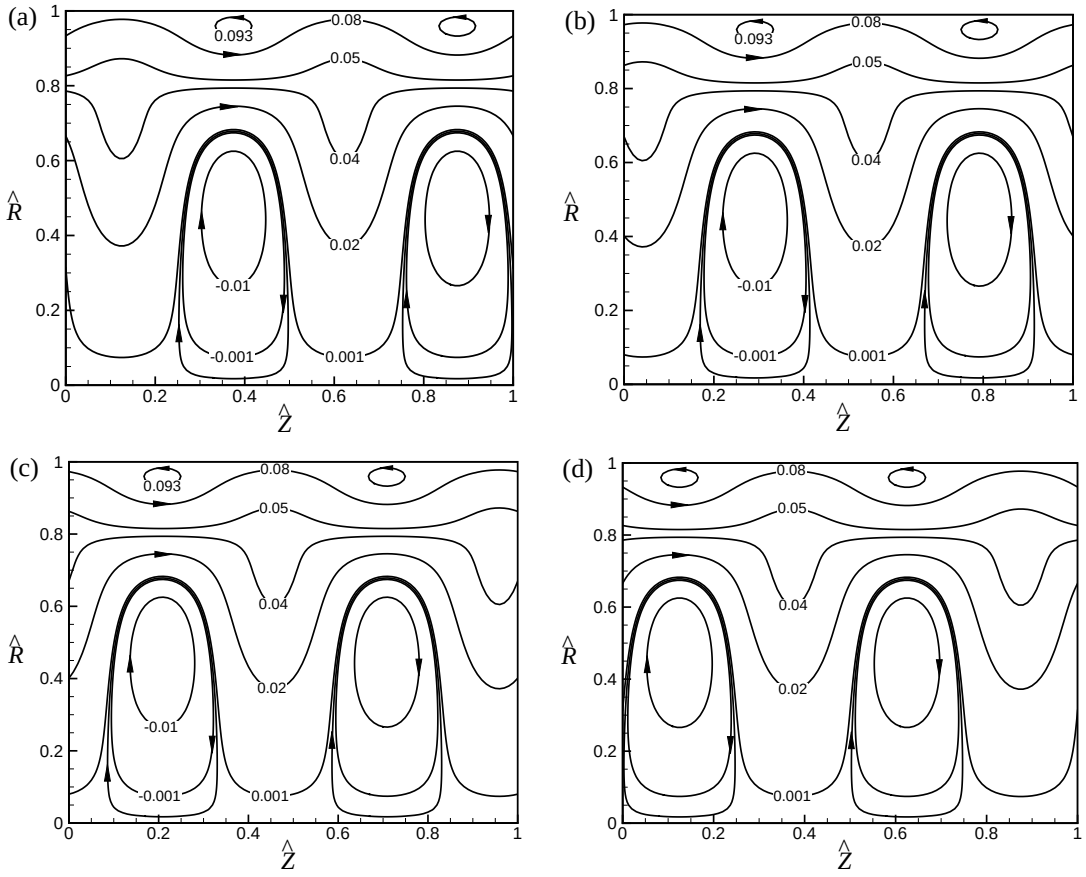

Figure 4: Effect of the phase angle of the backward wave: mass transport streamlines in partially standing waves in a partially obstructed tube ($Y = 0.5$), where $\hat{k} = 2\pi$, $\alpha = 20$, $S_r = 0.7$ and $\phi =$ (a) 0, (b) $\pi/3$ (c) $2\pi/3$, (d) π.

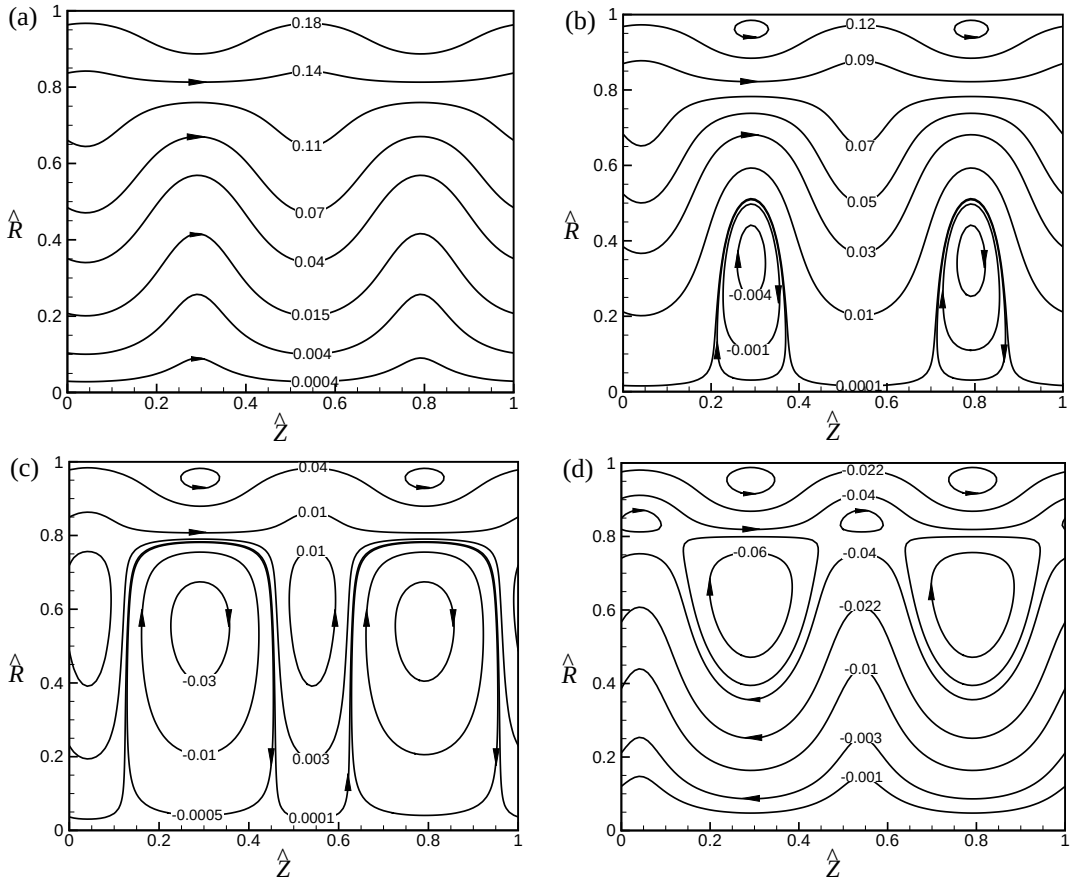

Figure 5: Effect of end obstruction: mass transport streamlines in partially standing waves ($S_r = 0.7$, $\phi = \pi/3$) in a partially obstructed tube, where $\hat{k} = 2\pi$, $\alpha = 20$ and $Y =$ (a) 0, (b) 0.3 (c) 0.7, (d) 1.0.

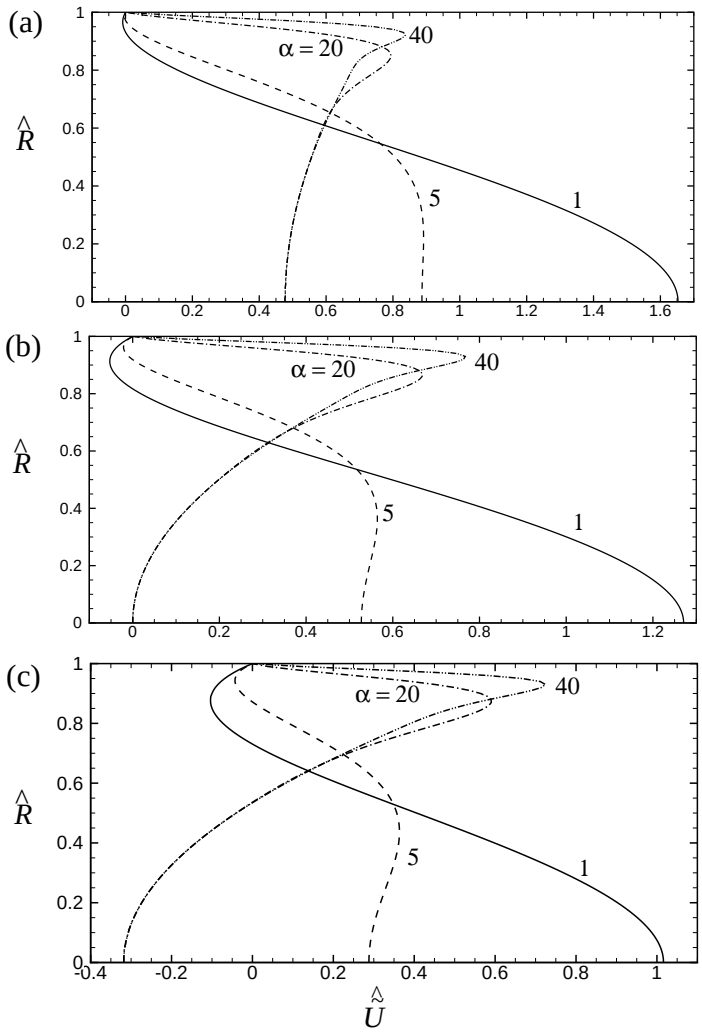

Figure 6: Steady axial velocity profiles $\hat{\hat{U}}(\hat{R})$ as a function of the Womersley number α, where $S_r = 0.0$ (progressive wave), $\hat{k} = 2\pi$ and $Y =$ (a) 0.2, (b) 0.5 (c) 0.7.